

# Atomic-scale Modeling of Self-Positioning Nanostructures

Y. Nishidate<sup>1</sup> and G. P. Nikishkov<sup>1,2</sup>

**Abstract:** Atomic-scale finite element procedure for modeling of self-positioning nanostructures is developed. Our variant of the atomic-scale finite element method is based on a meshless approach and on the Tersoff interatomic potential function. The developed algorithm is used for determination of equilibrium configuration of atoms after nanostructure self-positioning. Dependency of the curvature radius of nanostructures on their thickness is investigated. It is found that for thin nanostructures the curvature radius is considerably smaller than predicted by continuum mechanics equations. Curvature radius variation with varying orientation of crystallographic axes is also modeled and results are compared to finite element continuum anisotropic solution.

**Keyword:** Nanostructure, Self-positioning, Atomic-scale finite element method.

## 1 Introduction

Nanoscale structures have many potential applications. However, controlling and manipulating formation of nanoscale structures is usually complicated. One promising approach to creation of 3D nanoscale structures is the method utilizing self-positioning phenomena of thin solid films [Schmidt and Eberl (2001); Songmuang, Deneke, and Schmidt (2006); Golod, Prinz, Mashanov, and Gutakovskiy (2001); Vaccaro, Kubota, and Aida (2001)]. The self-positioning is caused by lattice mis-matching strain in layered structures composed of several metal or semiconductor materials. The self-positioning structures are created by depositing a sacrificial material layer and several lattice mismatched layers. After etching away the sacrificial layer, the layered materials

form hinges or tubes with diameter controllable by layer material properties and thickness. Strain-driven self-positioning can be used to create 3D nanoscale structures by folding 2D membranes as *origami* (Japanese paper craft work) [In, Kumar, Shao-Horn, and Barbastathis (2006); Arora, Nichol, Smith, and Barbastathis (2006)]. This approach is simple and robust, and deformation is predictable and controllable.

Analytical continuum mechanics approaches [Hsueh (2002); Nikishkov (2003); Nishidate and Nikishkov (2006)] and computational finite element modeling [Nikishkov, Khmyrova, and Ryzhii (2003); Nikishkov, Nishidate, Ohnishi, and Vaccaro (2006)] have been applied to estimating deformations of self-positioning multi-layer structures. However, these approaches do not take into account atomic-scale effects like absence of neighboring atoms at free surfaces.

Recently, atomic-scale modeling has been applied to practical systems consisting of hundreds of thousands of atoms [Fitzgerald, Goldbeck-Wood, Kung, Petersen, Subramanian, and Wescott (2008)]. Several finite element algorithms have been developed for multiscale simulations [Theodosiou and Saravanos (2007); Chirputkar and Qian (2008)]. The atomic-scale finite element method (AFEM) based on the Brenner interatomic potential has been proposed for multiscale analysis of carbon nanotubes [Liu, Huang, Jiang, Qu, and Hwang (2004); Liu, Jiang, Huang, Qu, Yu, and Hwang (2005)]. We have applied the AFEM to modeling of self-positioning bi-layer structures. The investigation of curvature radius dependence on the structure thickness [Nishidate and Nikishkov (2007)] showed that atomic-scale and continuum mechanics solutions produce same results for structures with thickness larger than 100 nm. Atomic scale effects play significant role for thin self-positioning nanostructures.

<sup>1</sup> University of Aizu, Aizu-Wakamatsu 965-8580, Japan

<sup>2</sup> Corresponding author, email: niki@u-aizu.ac.jp

In this article, formulation of the atomic-scale finite element method with the use of the Tersoff-Nordlund potential function is presented. Since the self-positioning of nanostructures involves large translations and rotations, a special iteration procedure that includes load relaxation factor is developed. The created AFEM code is applied to modeling of bi-layer self-positioning nanostructures. Deformation of self-positioning structures with varying thickness and with varying orientations of crystallographic axes is investigated.

## 2 Atomic-scale finite element method

The atomic-scale finite element method (AFEM) is proposed for analysis of carbon nanotubes [Liu, Huang, Jiang, Qu, and Hwang (2004); Liu, Jiang, Huang, Qu, Yu, and Hwang (2005)]. The atomic-scale finite element equation system is derived from the approximation of energy  $E$  around current configuration  $\mathbf{x}^{(i)}$ :

$$E(\mathbf{x}) \approx E(\mathbf{x}^{(i)}) + \frac{\partial E}{\partial \mathbf{x}} \Big|_{\mathbf{x}=\mathbf{x}^{(i)}} \cdot (\mathbf{x} - \mathbf{x}^{(i)}) + \frac{1}{2} (\mathbf{x} - \mathbf{x}^{(i)})^T \cdot \frac{\partial^2 E}{\partial \mathbf{x}^2} \Big|_{\mathbf{x}=\mathbf{x}^{(i)}} \cdot (\mathbf{x} - \mathbf{x}^{(i)}), \quad (1)$$

and its subsequent minimization:

$$\frac{\partial E}{\partial \mathbf{x}} = 0. \quad (2)$$

Substituting equation (1) into (2), AFEM global equation system can be obtained, and expressed in a form similar to conventional finite element equation system:

$$\mathbf{K}\mathbf{u} = \mathbf{f}, \quad (3)$$

where  $\mathbf{K}$  is a global stiffness matrix,  $\mathbf{u}$  is a displacement vector, and  $\mathbf{f}$  is a load (force) vector. In the AFEM, the global stiffness matrix  $\mathbf{K}$  and the load vector  $\mathbf{f}$  are composed of second and first derivatives of the system energy with respect to atom positions:

$$\mathbf{K} = \begin{bmatrix} \left( \frac{\partial^2 E}{\partial \mathbf{x}_1 \partial \mathbf{x}_1} \right)_{3 \times 3} & \cdots & \left( \frac{\partial^2 E}{\partial \mathbf{x}_1 \partial \mathbf{x}_n} \right)_{3 \times 3} \\ \vdots & \ddots & \vdots \\ \left( \frac{\partial^2 E}{\partial \mathbf{x}_n \partial \mathbf{x}_1} \right)_{3 \times 3} & \cdots & \left( \frac{\partial^2 E}{\partial \mathbf{x}_n \partial \mathbf{x}_n} \right)_{3 \times 3} \end{bmatrix}, \quad (4)$$

$$\mathbf{f} = \begin{Bmatrix} \left( -\frac{\partial E}{\partial \mathbf{x}_1} \right)_{1 \times 3} \\ \vdots \\ \left( -\frac{\partial E}{\partial \mathbf{x}_n} \right)_{1 \times 3} \end{Bmatrix}, \quad (5)$$

where  $E$  is the total energy of the atomic system,  $n$  is a number of atoms (AFEM nodes), and  $\mathbf{x}_i$  is the coordinate vector of an  $i$ -th atom. As long as the problem is to find the static equilibrium configuration of atomic bonds without external loads, total energy  $E$  is replaced by a potential energy. Expressions of energy derivatives should be obtained to formulate the AFEM global equation system, so energy function  $E$  should be at least twice differentiable.

Equation (1) shows that solution becomes less reliable as current configuration gets further from equilibrium atomic configuration. Self-positioning structures deform with large translational and rotational displacements, so it is desirable to divide loading into several steps and to apply load gradually. Therefore, we employ the following Newton-Raphson iteration procedure to obtain the final structure shape.

$$\begin{aligned} &\text{do} \\ &\quad \mathbf{K} = \mathbf{K}(\mathbf{x}^{(i)}) \\ &\quad \mathbf{f} = \mathbf{f}(\mathbf{x}^{(i)}) \\ &\quad \alpha = g(\mathbf{K}, \mathbf{f}) \\ &\quad \mathbf{f} = \alpha \mathbf{f}(\mathbf{x}^{(i)}) \\ &\quad \Delta \mathbf{u} = \mathbf{K}^{-1} \mathbf{f} \\ &\quad \mathbf{x}^{(i+1)} = \mathbf{x}^{(i)} + \Delta \mathbf{u} \\ &\quad u^{(i+1)} = u^{(i)} + |\Delta \mathbf{u}| \\ &\quad \text{while } \frac{|\Delta \mathbf{u}|}{u^{(i+1)}} > \varepsilon \end{aligned} \quad (6)$$

At each updated configuration, tangent stiffness matrix and loading vector should be calculated using equation (4) and (5). In the iteration procedure,  $\varepsilon$  is an error tolerance,  $g$  is a function for estimating load relaxation factor  $\alpha$ . Constant  $\alpha$  factor throughout overall solution can perform unnecessary iterations or can lead to divergence, because derivative (slope) of the interaction potential energy usually becomes smaller as current configuration gets closer to equilibrium where loading becomes zero.

The relaxation factor is estimated at each loading step using tangent stiffness matrix and current

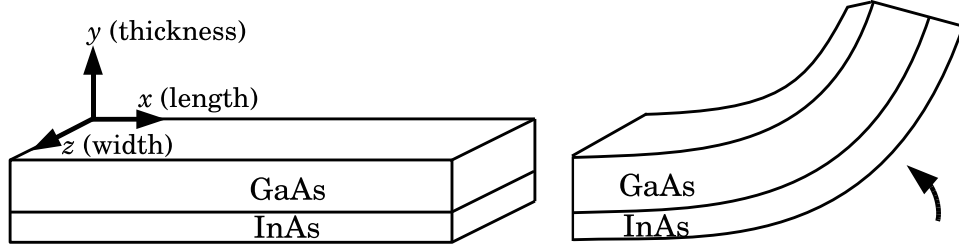


Figure 1: Self-positioning GaAs-InAs bi-layer hinge before and after self-positioning.

loading vector. In our case, the value of  $\alpha$  is calculated as:

$$u = \frac{u_{mean}}{a},$$

$$u_{mean} = \frac{1}{n} \sum_{i=0}^n \left| \left( \frac{f_1^i}{K_{11}^{ii}}, \frac{f_2^i}{K_{22}^{ii}}, \frac{f_3^i}{K_{33}^{ii}} \right) \right|, \quad (7)$$

$$\alpha = \begin{cases} 1, & u \leq \delta, \\ \frac{\delta}{u}, & u > \delta, \end{cases}$$

where  $n$  is a number of atoms,  $f_j^i$  is a  $j$ -th component of full load vector acting on  $i$ -th atom,  $K_{jj}^{ii}$  are corresponding diagonal entries of current tangent stiffness matrix,  $a$  is a characteristic length of atomic system, and  $\delta$  is a displacement suppression factor representing admissible mean displacement length. We selected characteristic length  $a$  as an initial lattice period, and a constant  $\delta$  with the value  $2 \cdot 10^{-4}$ . Stronger load relaxation is applied if smaller  $\delta$  is selected, or calculated mean value of the solution guess  $u_{mean}$  increases.

### 3 Modeling GaAs and InAs crystalline structures

We model bi-layer self-positioning hinges consisting of GaAs top and InAs lower layer (Fig. 1). Coordinate axes  $x$ ,  $y$ , and  $z$  are aligned to structure length, thickness, and width (bending axis) directions, respectively.

An AFEM mesh is constructed in accordance with GaAs and InAs crystalline structures called zincblende crystal. Arrangement of atoms in zincblende crystals is shown in Fig. 2. Arsenide atoms occupy crystal corners and face centers of the unit crystal, and Gallium/Indium atoms are inside with positions  $(0.25, 0.25, 0.25)$ ,  $(0.75, 0.25,$

$0.75)$ ,  $(0.25, 0.75, 0.75)$ , and  $(0.75, 0.75, 0.25)$  in the unit edge length crystal.

The GaAs and InAs possess material anisotropy depending on its crystal orientation. We investigate the effect of anisotropy depending on a material orientation angle. The material orientation angle is modeled by rotating crystals around global  $y$  axis. Fig. 3 shows the procedure of creation AFEM meshes for modeling GaAs and InAs material anisotropy. The original crystalline structure with zero material orientation angle is prepared. Then the structure is rotated around  $y$  axis and atoms outside the rectangular solution domain are removed.

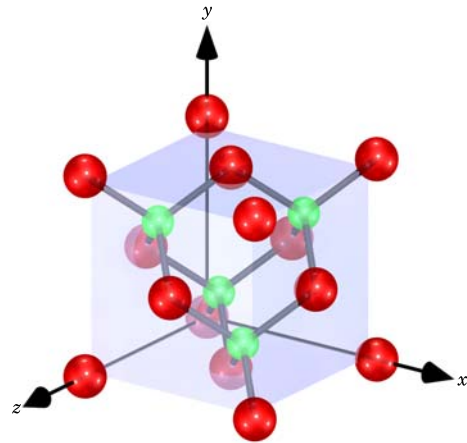


Figure 2: Atomic configuration and bonding in zincblende crystalline structures. There are eight corner and six face center atoms (bigger) and four inner atoms (smaller).

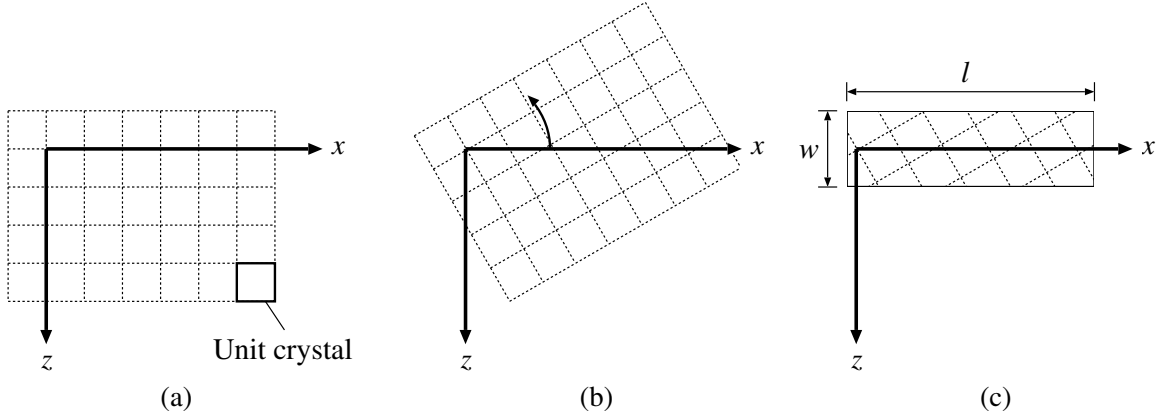


Figure 3: Modeling atomic structures with different material axes orientation. (a) Initial structure with unit crystals aligned to global axes. (b) Structure rotation around y axis by specified orientation angle. (c) Removal of atoms outside a rectangular region.

#### 4 Modeling In-Ga-As atomic interaction

The atomic-scale finite element method employs continuous empirical interatomic potential function which describes interatomic interactions. Several empirical interatomic potential functions have been developed to study behavior of atomic systems [Brenner (1990); Brenner, Shenderova, Harrison, Stuart, Ni, and Sinnott (2002); Tersoff (1989)]. For example, Liu, Huang, Jiang, Qu, and Hwang (2004); Liu, Jiang, Huang, Qu, Yu, and Hwang (2005) employed an empirical interatomic potential function and its parameters developed by Brenner (1990); Brenner, Shenderova, Harrison, Stuart, Ni, and Sinnott (2002).

Although the Brenner potential model is widely used and successfully applied for modeling several types of atomic structures, its parameters for Indium, Gallium, and Arsenide systems are not available. Another empirical potential energy model has been proposed by Tersoff (1989). In the Tersoff model, total potential energy  $E$  is given by the following function:

$$E = \sum_i E_i = \frac{1}{2} \sum_i \sum_{j \neq i} V_{ij},$$

$$V_{ij} = f_C(r_{ij}) [f_R(r_{ij}) + b_{ij} f_A(r_{ij})],$$

$$f_R(r_{ij}) = A_{ij} \exp(-\lambda_{ij} r_{ij}),$$

$$f_A(r_{ij}) = -B_{ij} \exp(-\mu_{ij} r_{ij}),$$

$$f_C(r_{ij}) = \begin{cases} 1, & r_{ij} \leq R_{ij}, \\ \frac{1}{2} + \frac{1}{2} \cos \left[ \frac{r_{ij} - R_{ij}}{S_{ij} - R_{ij}} \pi \right], & R_{ij} < r_{ij} < S_{ij}, \\ 0, & S_{ij} \leq r_{ij}, \end{cases}$$

$$b_{ij} = (1 + \beta_{ij}^{n_{ij}} \zeta_{ij}^{n_{ij}})^{-1/(2n_{ij})},$$

$$\zeta_{ij} = \sum_{k \neq i, j} f_C(r_{ik}) g(\theta_{ijk}),$$

$$g(\theta_{ijk}) = 1 + \frac{c_{ik}^2}{d_{ik}^2} - \frac{c_{ik}^2}{d_{ik}^2 + (h_{ik} - \cos \theta_{ijk})^2}, \quad (8)$$

where  $E_i$  is the potential energy of atom  $i$ ,  $V_{ij}$  the potential energy of a bond  $i-j$ ,  $r_{ij}$  the distance from atom  $i$  to atom  $j$ ,  $f_C$  the cut-off function to disregard effects from distant atoms,  $f_R$  a reactive component,  $f_A$  an attractive component, and  $b_{ij}$  a bonding term to represent multi-atom interaction effects characterized by bonding angles.

Appearance of the potential function (8) is slightly different from the original Tersoff potential function due to subsequent parametrization by Nordlund, Nord, Frantz, and Keinonen (2000) for Indium, Gallium and Arsenide systems. The parameter values for Indium, Gallium, and Arsenide systems are listed in Tab. 1.

The parameters obtained by Nordlund correspond to basic elastic and melting crystal properties. They were developed for investigation of damage at Si/Ge, AlAs/GaAs, and InAs/GaAs interfaces. It was noted that the parameters should be used with care for other purposes. So, we performed

Table 1: Tersoff potential energy parameters for Indium, Gallium, and Arsenide systems fit by Nordlund, Nord, Frantz, and Keinonen (2000)

	In–Ga	In–In	In–As	As–As	Ga–As	Ga–Ga
$n$	3.43739	3.40223	0.7561694	0.60879133	6.31741	3.4729041
$c$	0.0801587	0.084215	5.172421	5.273131	1.226302	0.07629773
$d$	19.5277	19.2626	1.665967	0.75102662	0.790396	19.796474
$h$	7.26805	7.39228	-0.5413316	0.15292354	-0.518489	7.1459174
$\beta$	0.705241	2.10871	0.3186402	0.00748809	0.357192	0.23586237
$\lambda$ ( $^{-1}$ )	2.5616	2.6159	2.597556	2.384132239	2.82809263	2.50842747
$\mu$ ( $^{-1}$ )	1.58314	1.68117	1.422429	1.7287263	1.72301158	1.490824
$A$ (eV)	1719.7	2975.54	1968.295443	1571.86084	2543.29720	993.888094
$B$ (eV)	221.557	360.61	266.571631	546.4316579	314.459660	136.123032
$R$ ()	3.4	3.5	3.5	3.4	3.4	3.4
$S$ ()	3.6	3.7	3.7	3.6	3.6	3.6

several tests to confirm parameter suitability for our modeling of self-positioning structures. The first test measured correspondence of elastic properties obtained using the Nordlund parameters to elastic properties known from the literature. The second test involved calculation of lattice parameters for GaAs and InAs and their comparison to known values.

Using the AFEM with Tersoff potential and Nordlund parameters, elastic properties of GaAs and InAs are estimated by applying external load at the end of specimen shaped into a thin rod along its longitudinal direction. Strain and stress are calculated at a position sufficiently far from the free end where external load is applied. Taking into account that the specimen is thin in transverse directions, Young's modulus  $E$  and Poisson's ratio  $\nu$  are determined by:

$$E = \frac{\sigma_x}{\epsilon_x}, \quad \nu = -\frac{\epsilon_y}{\epsilon_x}. \quad (9)$$

For a cubic crystal with axes aligned with cube edges, estimation of Young's modulus and Poisson's ratio from constitutive tensor components  $C_{11}$  and  $C_{12}$  can be made as follows:

$$E = \frac{(C_{11} - C_{12})(C_{11} + 2C_{12})}{C_{11} + C_{12}}, \quad \nu = \frac{C_{12}}{C_{11} + C_{12}}. \quad (10)$$

The lattice period is estimated at the center of cube structures consisting of several crystals in

all directions. Elastic properties and lattice periods estimated by the AFEM modeling for GaAs and InAs are compared with experimental values [Bhattacharya (1993)] in Tab. 2.

A difference of 5% is observed for Young's modulus of GaAs, however in general the correspondence of estimated elastic properties to their experimental values is acceptable. Estimated lattice periods are in very good agreement with experimental values. We therefore concluded that the AFEM with Tersoff potential and parameters developed by Nordlund is suitable for simulation of the atomic-scale behaviour of nanostructures composed of GaAs and InAs.

## 5 Modeling self-positioning GaAs–InAs hinges

A self-positioning structure consisting of GaAs top and InAs lower layers is shown in Fig. 4. It is used for investigation of curvature radius dependence on structure thickness and crystal orientation angle. We employ problem size parameter  $c$  to express size of atomic systems. Curvature radius of GaAs and InAs bilayer structures with the problem size parameters  $c = 1, 2, 4, 8, 12, 16, 24,$  and  $36$  prepared to find equilibrium configuration. We model material anisotropy with material orientation angles  $0, 15, 30, 45, 60, 75,$  and  $90$  degrees. Appearance of crystalline structure ge-

Table 2: GaAs and InAs properties: comparison of AFEM estimation with literature [Bhattacharya (1993)].

	GaAs			InAs		
	Experiment	AFEM	$\delta$ (%)	Experiment	AFEM	$\delta$ (%)
$E$ (GPa)	85.3	81.0	-5.04	51.8	51.4	-0.77
$\nu$	0.312	0.313	0.32	0.352	0.357	1.42
LP (nm)	0.56533	0.56389	-0.25	0.60584	0.60592	0.01

ometry is shown in Fig. 5 for varying orientation angles.

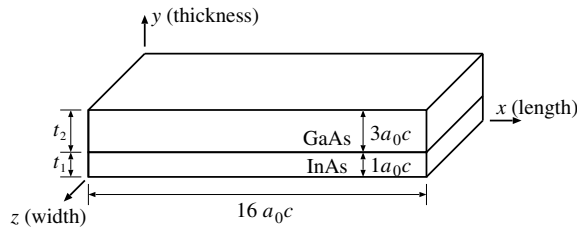


Figure 4: Schematic of a self-positioning problem. The number of atoms in the problem is determined by the parameter  $c$ .

The top GaAs and lower InAs layer are composed of  $3c$  and  $c$  number of crystals in the thickness ( $y$ ) direction. In the length ( $x$ ) direction, several atomic layers of length  $16a_0c$  is prepared where  $a_0$  is an initial lattice period (Fig. 4). For hinge with  $0$  orientation angle,  $16a_0c$  is equals to length of 16 unit crystals.

We compare results obtained by AFEM with analytical continuum mechanics solution under plane strain conditions [Nikishkov (2003)]. The plane strain conditions correspond to structures with infinite width in  $z$  direction. In order to simulate atomic systems of infinite dimensions, periodic boundary conditions, which help to minimize number of atoms in the model are usually employed in computational modeling.

Periodic boundary conditions in the  $z$  (width) direction are applied for structures with orientation angles  $0$ ,  $45$  and  $90$  degrees. Such structures consist of one complete and another incomplete crystal in the width direction, and connection across periodic boundary is created when looking for neighboring atoms.

For hinges with the other orientation angles ( $15$ ,  $30$ ,  $60$  and  $75$  degrees), enough number of atomic layers corresponding to width  $30a_0$  are prepared and displacement is constrained in the width direction to imitate plane strain conditions ( $\epsilon_z = 0$ ). Boundary condition restricting displacements in  $x$  direction at one end of the structure are also applied.

The analytical continuum mechanics solution is used for comparison. In addition, in order to reduce computing time, the initial configuration of atoms in AFEM meshes is determined according to the curvature radius given by continuum mechanics solution under plane strain conditions [Nikishkov (2003)]:

$$R = \frac{E_1'^2 t_1^4 + E_2'^2 t_2^4 + 2E_1' E_2' t_1 t_2 (2t_1^2 + 2t_2^2 + 3t_1 t_2)}{6E_1' E_2' t_1 t_2 (t_1 + t_2) (\eta_1 \epsilon_1^0 - \eta_2 \epsilon_2^0)},$$

$$E_i' = \frac{E_i}{1 - \nu_i^2}, \quad \eta_i = 1 + \nu_i,$$
(11)

where  $E_i$ ,  $\nu_i$ ,  $t_i$ , and  $\epsilon_i^0$  are Young's modulus, Poisson's ratio, thickness, and initial lattice mismatching strain, respectively. Subscripts 1 and 2 denote material layers. In bi-layer systems, expression is symmetric to each other, so distinction of layer 1 and 2 for curvature radius calculation is not important.

Definition of thickness for structures consisting of just a few crystal layers in the thickness direction should be done with care when calculating curvature radius using an analytical technique. It is appropriate to add some offset equal to a 'radius' of an atom at each free surface. While adding such an offset is not critical for thick structures, it can be important for problems with small number of crystals in  $y$  direction.

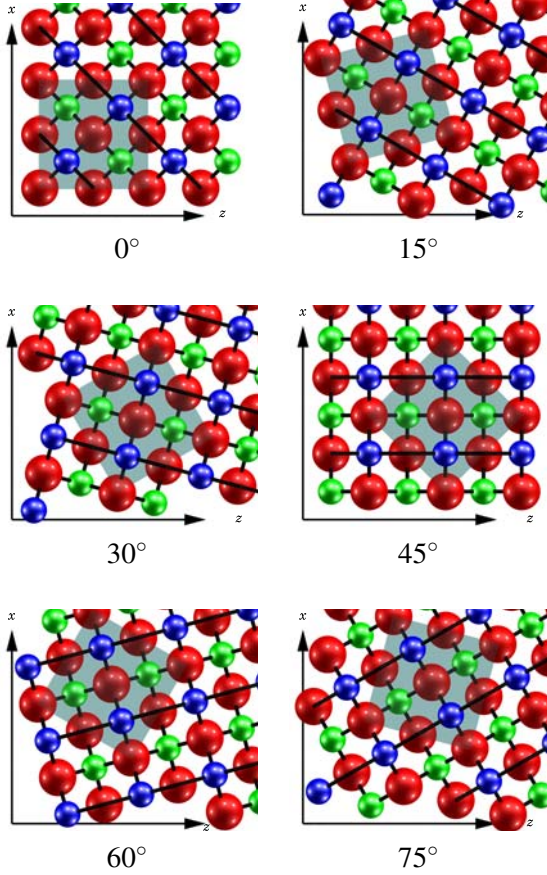


Figure 5: Top view of atom configurations for self-positioning hinges with different orientation angles. Orientation angles 0, 45, and 90 degrees have periodic boundary in  $z$  (width) direction.

If we adopt half of the atom connectivity length as an offset, then for zincblende crystal structures the offset is equal to  $\sqrt{3}a/8$ , where  $a$  is a lattice period. Corresponding offsets are 0.1224 nm for GaAs and 0.1425 nm for InAs.

Initial strains  $\epsilon_i^0$  in equation (11) are determined by initial ( $a_0$ ) and material-specific lattice period ( $a_i$ ) as:

$$\epsilon_i^0 = \frac{a_i - a_0}{a_0}. \quad (12)$$

We determine the initial lattice period for the bi-layer system using a weighted linear interpolation of GaAs and InAs specific lattice periods:

$$a_0 = \frac{a_1 n_1 + a_2 n_2}{n_1 + n_2}, \quad (13)$$

where  $n_1$  and  $n_2$  are number of crystals in each InAs and GaAs layer. Therefore,  $a_0$  is assumed to be 0.57546 nm in our problems.

## 6 Numerical results

The developed AFEM computer program was used to solve two problem series for self-positioning nanostructures. The first one is computing the curvature radius of bi-layer hinges with varying thickness. The second series includes problems with varying orientation of material axes for the same nanostructures.

### 6.1 Curvature dependence on the structure thickness

Bi-layer atomic structures of different thickness are created by setting problem size parameter  $c$  to 1, 2, 4, 8, 12, 16, 24, and 36. Corresponding thicknesses are 2.56, 4.86, 9.46, 18.65, 27.84, 37.03, 55.41 and 82.98 nm. The equilibrium configurations of bi-layer hinges are determined with the use of Newton-Raphson iteration procedure (6). We compare the AFEM values of curvature radius with the continuum mechanics solution under plane strain conditions [Nikishkov (2003)]. In the continuum mechanics solution, elastic properties estimated by the AFEM on the tensile rod model are used (see Tab. 2).

Curvature radius values based on the AFEM modeling at the top and at the bottom of the atomic structures are calculated by taking three neighbor nodes along the  $x$  direction to fit a circle at each  $y$  level. Then, these values are used to calculate curvature radius at the neutral layer by linear interpolation. The neutral layer is located at 0.54 of the thickness from the bottom of the structure in our problems.

Fig. 6 shows the final shape of an atomic model after self-positioning in case of problem size  $c = 1$ , totally four unit crystals in the thickness direction. Analysis reveals that spacing of atoms is smaller in GaAs and larger in InAs, and that the free end is not straight along local thickness direction, due to expansion in the lower layer and compression in the top layer.

In order to estimate convergence of the curvature

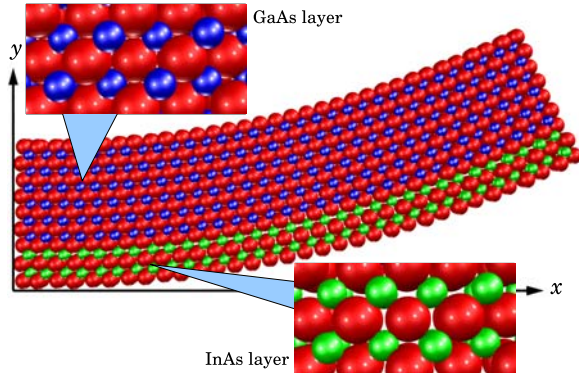


Figure 6: Final shape of atomic bi-layer structure with the size  $c = 1$ .

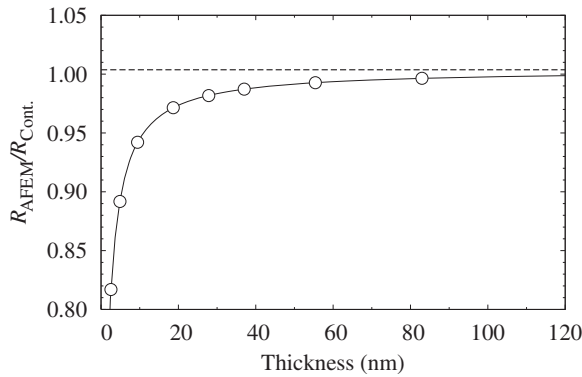


Figure 7: Ratio of the curvature radius determined by the AFEM and the continuum mechanics solution with varying thickness.

radius with thickness increase, least square fits of the obtained eight numerical solutions are performed using power function  $R(c) = \alpha_1 (\alpha_2 c + \alpha_3)^{-\beta} + \gamma$ , where  $c$  indicates size of the atomic system, and  $\alpha_1$ ,  $\alpha_2$ ,  $\alpha_3$ ,  $\beta$ , and  $\gamma$  are parameters found by least square fit, where  $\gamma$  corresponds to converged value for infinite number of crystal layers. Fig. 7 shows the ratio of the curvature radius determined by the AFEM and the continuum mechanics solution with varying thickness.

Least square fits indicate that the relative difference of curvature radius converges to 1.0037 for an infinite number of atomic layers. For the biggest problem we investigated ( $c = 36$ ), the difference is  $-0.36\%$ . So, the AFEM and continuum mechanics solution are in quite good agree-

ment for large thickness. The difference between atomic-scale and continuum mechanics curvature radius increases with reduction of the structure thickness. This difference is  $-18.4\%$  for  $c = 1$ , corresponding to four unit crystals in the thickness direction and thickness 2.56 nm.

## 6.2 Curvature dependence on the material orientation angle

AFEM solutions with problem sizes  $c = 1, 2, 4$  and 8 and material orientation angles 0, 15, 30, 45, 60, 75 and 90 degrees are performed for modeling anisotropy of GaAs and InAs bi-layer nanostructures. Fig. 8 shows the final shape of atomic models after self-positioning in case of crystal size  $c = 1$  for orientation angles 0, 15, 30, 45, 60 and 75 degrees.

Tab. 3 contains ratios of the curvature radius  $R$  to the thickness  $t$  obtained by the AFEM modeling at the neutral layer for orientation angles 0, 15, 30 and 45 degrees and by continuum mechanics solution for zero orientation angle. For varying orientation angles, the ratio in between maximum and minimum values of curvature radius is about 1.35. This ratio is similar to experimental data and numerical finite element modeling of GaAs and  $\text{In}_{0.2}\text{Ga}_{0.8}\text{As}$  bi-layer structures [Nikishkov, Nishidate, Ohnishi, and Vaccaro (2006)]

Fig. 9 shows dependency of the curvature radius ratio ( $R_{AFEM}/R_{Cont.(0^\circ)}$ ) for varying material orientation angle. Curvature radius is the minimum at orientation angles 0 and 90 degrees and maximum at 45 degrees, and dependency on orientation angle shows a curve similar to sinusoidal function with frequency  $\pi$ .

## 7 Conclusion

Algorithm of the atomic-scale finite element method based on the Tersoff interatomic potential has been developed. Solution procedure for problems with large displacements is organized as the Newton-Raphson iteration procedure. A load relaxation factor is introduced in order to restrict load step magnitude for cases with high gradients of the atomic system energy.

The developed AFEM code is applied to modeling

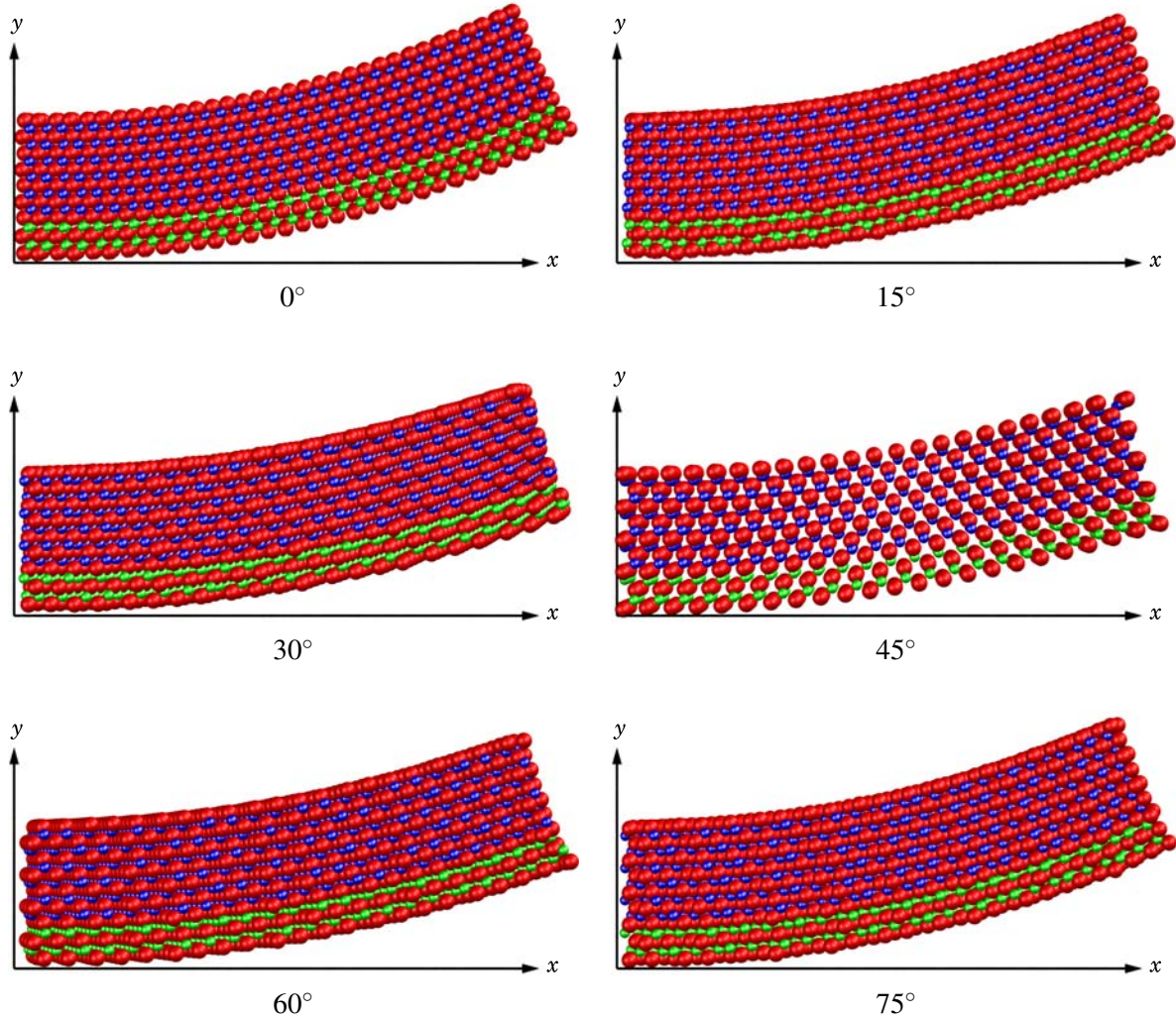


Figure 8: Final shape of atomic bi-layer structure with the size  $c = 1$  for orientation angles 0 to 75 degrees.

of GaAs and InAs bi-layer self-positioning nanostructures. Two problem series include investigation nanohinge curvature radius dependence on the structure thickness and the material orientation angle. The self-positioning hinge deformation converges to the continuum mechanics solution under plane strain conditions with increasing structure thickness. However, for nanostructures of small thickness less than 40 nm atomic-scale effects play considerable role. Dependency of curvature radius on the material orientation angle shows periodic curve with the maximum curvature radius observed for orientation angle 45 degrees. Our modeling shows that hinges with different material orientation angles can exhibit curvature radius differing by 35%.

#### Appendix A: First order differentiation of Tersoff potential for calculation of force vector

Tersoff potential function (8) is used to estimate forces acting on each atom. Assembly of first order derivatives of bonding  $i$ - $j$  energy  $V_{ij}$  yields the global force vector. Let the distance  $r_{ij}$  between atoms with positions  $\mathbf{x}_i$  and  $\mathbf{x}_j$  is defined as:

$$r_{ij} = |\mathbf{r}_{ij}| = |\mathbf{x}_j - \mathbf{x}_i|$$

Then derivatives of  $r_{ij}$  in respect to atom positions  $\mathbf{x}_i$  and  $\mathbf{x}_j$  are:

$$\frac{\partial r_{ij}}{\partial \mathbf{x}_i} = -\frac{\mathbf{x}_j - \mathbf{x}_i}{r_{ij}}$$

Table 3: Total thickness  $t$  (nm) and relative value of curvature radius  $R/t$  for problem sizes  $c = 1, 2, 4$  and 8 with varying orientation angles. Dependency on orientation angle is symmetric in respect to orientation angle 45 degree.

$c$	$t$ (nm)	Cont. ( $0^\circ$ )	AFEM ( $0^\circ$ )	AFEM ( $15^\circ$ )	AFEM ( $30^\circ$ )	AFEM ( $45^\circ$ )
1	2.56	9.25	7.56	8.32	9.86	10.67
2	4.86	9.60	8.56	9.35	10.88	11.76
4	9.46	9.81	9.23	9.98	11.54	12.54
8	18.65	9.92	9.63	10.29	11.87	13.01

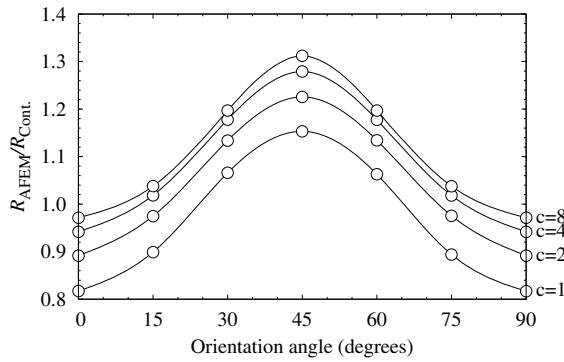


Figure 9: Dependency of  $R_{AFEM}/R_{Cont.(0^\circ)}$  on orientation angle for problem sizes  $c = 1$  to 8.

$$\frac{\partial r_{ij}}{\partial \mathbf{x}_j} = \frac{\mathbf{x}_j - \mathbf{x}_i}{r_{ij}}$$

Differentiation of  $V_{ij}$  in respect to positions  $\mathbf{x}_i$ ,  $\mathbf{x}_j$ , and any neighboring atom position  $\mathbf{x}_k$  yields:

$$\begin{aligned} \frac{\partial V_{ij}}{\partial \mathbf{x}_i} = & \frac{\partial r_{ij}}{\partial \mathbf{x}_i} \left[ \frac{\partial f_C}{\partial r_{ij}} \{f_R + b_{ij} f_A\} + f_C \left\{ \frac{\partial f_R}{\partial r_{ij}} + b_{ij} \frac{\partial f_A}{\partial r_{ij}} \right\} \right] \\ & + f_C f_A \frac{\partial b_{ij}}{\partial \mathbf{x}_i} \end{aligned}$$

$$\begin{aligned} \frac{\partial V_{ij}}{\partial \mathbf{x}_j} = & \frac{\partial r_{ij}}{\partial \mathbf{x}_j} \left[ \frac{\partial f_C}{\partial r_{ij}} \{f_R + b_{ij} f_A\} + f_C \left\{ \frac{\partial f_R}{\partial r_{ij}} + b_{ij} \frac{\partial f_A}{\partial r_{ij}} \right\} \right] \\ & + f_C f_A \frac{\partial b_{ij}}{\partial \mathbf{x}_j} \end{aligned}$$

$$\frac{\partial V_{ij}}{\partial \mathbf{x}_k} = f_C f_A \frac{\partial b_{ij}}{\partial \mathbf{x}_k}$$

Derivatives of  $b_{ij}$  in respect to positions  $\mathbf{x}_i$ ,  $\mathbf{x}_j$ , and  $\mathbf{x}_k$  have same appearance for all cases and is expressed as:

$$\frac{\partial b_{ij}}{\partial \mathbf{x}_i} = -\frac{1}{2} \beta^n \zeta_{ij}^{n-1} \frac{\partial \zeta_{ij}}{\partial \mathbf{x}_i} (1 + \beta^n \zeta_{ij}^n)^{-\frac{1}{2n}-1}$$

Differentiation of  $\zeta_{ij}$  in respect to positions  $\mathbf{x}_i$ ,  $\mathbf{x}_j$ , and  $\mathbf{x}_k$ :

$$\begin{aligned} \frac{\partial \zeta_{ij}}{\partial \mathbf{x}_i} = & \frac{\partial r_{ik}}{\partial \mathbf{x}_i} \frac{\partial f_C}{\partial r_{ik}} g(\theta_{ijk}) + f_C \frac{\partial \cos(\theta_{ijk})}{\partial \mathbf{x}_i} \frac{\partial g(\theta_{ijk})}{\partial \cos(\theta_{ijk})} \end{aligned}$$

$$\frac{\partial \zeta_{ij}}{\partial \mathbf{x}_j} = f_C \frac{\partial \cos(\theta_{ijk})}{\partial \mathbf{x}_j} \frac{\partial g(\theta_{ijk})}{\partial \cos(\theta_{ijk})}$$

$$\begin{aligned} \frac{\partial \zeta_{ij}}{\partial \mathbf{x}_k} = & \frac{\partial r_{ik}}{\partial \mathbf{x}_k} \frac{\partial f_C}{\partial r_{ik}} g(\theta_{ijk}) + f_C \frac{\partial \cos(\theta_{ijk})}{\partial \mathbf{x}_k} \frac{\partial g(\theta_{ijk})}{\partial \cos(\theta_{ijk})} \end{aligned}$$

Differentiation of  $\cos(\theta_{ijk})$  in respect to positions  $\mathbf{x}_i$ ,  $\mathbf{x}_j$ , and  $\mathbf{x}_k$ :

$$\begin{aligned} \frac{\partial \cos(\theta_{ijk})}{\partial \mathbf{x}_i} = & \frac{1}{(r_{ij} r_{ik})^2} \\ & \left[ \frac{\partial \mathbf{r}_{ij} \cdot \mathbf{r}_{ik}}{\partial \mathbf{x}_i} r_{ij} r_{ik} - (\mathbf{r}_{ij} \cdot \mathbf{r}_{ik}) \left\{ \frac{\partial r_{ij}}{\partial \mathbf{x}_i} r_{ik} + r_{ij} \frac{\partial r_{ik}}{\partial \mathbf{x}_i} \right\} \right] \end{aligned}$$

$$\frac{\partial \cos(\theta_{ijk})}{\partial \mathbf{x}_j} = \frac{1}{r_{ij}^2 r_{ik}} \left[ \frac{\partial \mathbf{r}_{ij} \cdot \mathbf{r}_{ik}}{\partial \mathbf{x}_j} r_{ij} - (\mathbf{r}_{ij} \cdot \mathbf{r}_{ik}) \frac{\partial r_{ij}}{\partial \mathbf{x}_j} \right]$$

$$\frac{\partial \cos(\theta_{ijk})}{\partial \mathbf{x}_k} = \frac{1}{r_{ij}^2 r_{ik}^2} \left[ \frac{\partial \mathbf{r}_{ij} \cdot \mathbf{r}_{ik}}{\partial \mathbf{x}_k} r_{ik} - (\mathbf{r}_{ij} \cdot \mathbf{r}_{ik}) \frac{\partial r_{ik}}{\partial \mathbf{x}_k} \right]$$

where  $\mathbf{r}_{ij} \cdot \mathbf{r}_{ik}$  denotes inner product of vectors  $\mathbf{r}_{ij}$  and  $\mathbf{r}_{ik}$ . Differentiation of  $\mathbf{r}_{ij} \cdot \mathbf{r}_{ik}$  in respect to  $\mathbf{x}_i$ ,  $\mathbf{x}_j$ , and  $\mathbf{x}_k$ :

$$\frac{\partial \mathbf{r}_{ij} \cdot \mathbf{r}_{ik}}{\partial \mathbf{x}_i} = -\{(\mathbf{x}_k - \mathbf{x}_i) + (\mathbf{x}_j - \mathbf{x}_i)\}$$

$$\frac{\partial \mathbf{r}_{ij} \cdot \mathbf{r}_{ik}}{\partial \mathbf{x}_j} = (\mathbf{x}_k - \mathbf{x}_i)$$

$$\frac{\partial \mathbf{r}_{ij} \cdot \mathbf{r}_{ik}}{\partial \mathbf{x}_k} = (\mathbf{x}_j - \mathbf{x}_i)$$

Differentiation of  $g(\theta_{ijk})$  in respect to  $\cos(\theta_{ijk})$ :

$$\frac{\partial g(\theta_{ijk})}{\partial \cos(\theta_{ijk})} = \frac{2c^2 \{h - \cos(\theta_{ijk})\}}{\left[ d^2 + \{h - \cos(\theta_{ijk})\}^2 \right]^2}$$

These are differentiations in respect to atom positions. In addition to these expressions, derivatives of  $f_C$ ,  $f_A$ ,  $f_R$  in respect to corresponding distances like  $r_{ij}$  or  $r_{ik}$  should be given.

## Appendix B: Second order differentiation of Tersoff potential for calculation of tangent stiffness matrix

The second order differentiation of Tersoff potential is calculated from first order differentiation. In second order differentiation, differentiation is calculated twice, so we employ superscript symbol to distinguish which is first or second differentiation symbol as following:

$\mathbf{x}_i^m$  first differentiation symbol  
 $\mathbf{x}_i^n$  second differentiation symbol

Second order differentiation of  $r_{ij}$  in respect to atom positions  $\mathbf{x}_i$  and  $\mathbf{x}_j$  are:

$$\frac{\partial^2 r_{ij}}{\partial \mathbf{x}_i^m \partial \mathbf{x}_i^n} = \begin{cases} \frac{1}{r_{ij}} - \frac{(\mathbf{x}_j - \mathbf{x}_i)^2}{r_{ij}^3} & \mathbf{x}_i^m = \mathbf{x}_i^n \\ -\frac{(\mathbf{x}_j - \mathbf{x}_i)^m (\mathbf{x}_j - \mathbf{x}_i)^n}{r_{ij}^3} & \mathbf{x}_i^m \neq \mathbf{x}_i^n \end{cases}$$

$$\frac{\partial^2 r_{ij}}{\partial \mathbf{x}_i^m \partial \mathbf{x}_j^n} = \frac{\partial^2 r_{ij}}{\partial \mathbf{x}_j^m \partial \mathbf{x}_i^n} =$$

$$\begin{cases} -\frac{1}{r_{ij}} + \frac{(\mathbf{x}_j - \mathbf{x}_i)^2}{r_{ij}^3} & \mathbf{x}_i^m = \mathbf{x}_j^n \\ \frac{(\mathbf{x}_j - \mathbf{x}_i)^m (\mathbf{x}_j - \mathbf{x}_i)^n}{r_{ij}^3} & \mathbf{x}_i^m \neq \mathbf{x}_j^n \end{cases}$$

For example,  $\mathbf{x}_i^m$  equals to  $\mathbf{x}_i^n$  when first differentiation symbol is  $x_i$  and second is  $x_i$ , but not equal when first differentiation symbol is  $x_i$  and second is  $y_i$ .

Differentiation of  $V_{ij}$  in respect to positions  $\mathbf{x}_i$ ,  $\mathbf{x}_j$ , and  $\mathbf{x}_k$ :

$$\begin{aligned} \frac{\partial^2 V_{ij}}{\partial \mathbf{x}_i^m \partial \mathbf{x}_i^n} &= \frac{\partial^2 r_{ij}}{\partial \mathbf{x}_i^m \partial \mathbf{x}_i^n} \\ &+ \left[ \frac{\partial f_C}{\partial r_{ij}} \{f_R + b_{ij} f_A\} + f_C \left\{ \frac{\partial f_R}{\partial r_{ij}} + b_{ij} \frac{\partial f_A}{\partial r_{ij}} \right\} \right] + \\ &\frac{\partial r_{ij}}{\partial \mathbf{x}_i^m} \frac{\partial r_{ij}}{\partial \mathbf{x}_i^n} \left[ \frac{\partial^2 f_C}{\partial r_{ij}^2} f_R + 2 \frac{\partial f_C}{\partial r_{ij}} \frac{\partial f_R}{\partial r_{ij}} + f_C \frac{\partial^2 f_R}{\partial r_{ij}^2} + \right. \\ &b_{ij} \left. \left\{ \frac{\partial^2 f_C}{\partial r_{ij}^2} f_A + 2 \frac{\partial f_C}{\partial r_{ij}} \frac{\partial f_A}{\partial r_{ij}} + f_C \frac{\partial^2 f_A}{\partial r_{ij}^2} \right\} \right] + \\ &\left( \frac{\partial r_{ij}}{\partial \mathbf{x}_i^m} \frac{\partial b_{ij}}{\partial \mathbf{x}_i^n} + \frac{\partial b_{ij}}{\partial \mathbf{x}_i^m} \frac{\partial r_{ij}}{\partial \mathbf{x}_i^n} \right) \left( \frac{\partial f_C}{\partial r_{ij}} f_A + f_C \frac{\partial f_A}{\partial r_{ij}} \right) + \\ &f_C f_A \frac{\partial^2 b_{ij}}{\partial \mathbf{x}_i^m \partial \mathbf{x}_i^n} \end{aligned}$$

$$\begin{aligned} \frac{\partial^2 V_{ij}}{\partial \mathbf{x}_i \partial \mathbf{x}_j} &= \frac{\partial^2 r_{ij}}{\partial \mathbf{x}_i \partial \mathbf{x}_j} \\ &+ \left[ \frac{\partial f_C}{\partial r_{ij}} \{f_R + b_{ij} f_A\} + f_C \left\{ \frac{\partial f_R}{\partial r_{ij}} + b_{ij} \frac{\partial f_A}{\partial r_{ij}} \right\} \right] + \\ &\frac{\partial r_{ij}}{\partial \mathbf{x}_i} \frac{\partial r_{ij}}{\partial \mathbf{x}_j} \left[ \frac{\partial^2 f_C}{\partial r_{ij}^2} f_R + 2 \frac{\partial f_C}{\partial r_{ij}} \frac{\partial f_R}{\partial r_{ij}} + f_C \frac{\partial^2 f_R}{\partial r_{ij}^2} + \right. \\ &b_{ij} \left. \left\{ \frac{\partial^2 f_C}{\partial r_{ij}^2} f_A + 2 \frac{\partial f_C}{\partial r_{ij}} \frac{\partial f_A}{\partial r_{ij}} + f_C \frac{\partial^2 f_A}{\partial r_{ij}^2} \right\} \right] + \end{aligned}$$

$$\left(\frac{\partial r_{ij}}{\partial \mathbf{x}_i} \frac{\partial b_{ij}}{\partial \mathbf{x}_j} + \frac{\partial b_{ij}}{\partial \mathbf{x}_i} \frac{\partial r_{ij}}{\partial \mathbf{x}_j}\right) \left(\frac{\partial f_C}{\partial r_{ij}} f_A + f_C \frac{\partial f_A}{\partial r_{ij}}\right) + f_C f_A \frac{\partial^2 b_{ij}}{\partial \mathbf{x}_j \partial \mathbf{x}_k} + f_C f_A \frac{\partial^2 b_{ij}}{\partial \mathbf{x}_i \partial \mathbf{x}_j}$$

$$\frac{\partial^2 V_{ij}}{\partial \mathbf{x}_i \partial \mathbf{x}_k} = \frac{\partial r_{ij}}{\partial \mathbf{x}_i} \frac{\partial b_{ij}}{\partial \mathbf{x}_k} \left(\frac{\partial f_C}{\partial r_{ij}} f_A + f_C \frac{\partial f_A}{\partial r_{ij}}\right) + f_C f_A \frac{\partial^2 b_{ij}}{\partial \mathbf{x}_k \partial \mathbf{x}_i} + f_C f_A \frac{\partial^2 b_{ij}}{\partial \mathbf{x}_i \partial \mathbf{x}_k}$$

$$\frac{\partial^2 V_{ij}}{\partial \mathbf{x}_j \partial \mathbf{x}_i} = \frac{\partial^2 r_{ij}}{\partial \mathbf{x}_j \partial \mathbf{x}_i}$$

$$\left[\frac{\partial f_C}{\partial r_{ij}} \{f_R + b_{ij} f_A\} + f_C \left\{\frac{\partial f_R}{\partial r_{ij}} + b_{ij} \frac{\partial f_A}{\partial r_{ij}}\right\}\right] + \frac{\partial r_{ij}}{\partial \mathbf{x}_j} \frac{\partial r_{ij}}{\partial \mathbf{x}_i} \left[\frac{\partial^2 f_C}{\partial r_{ij}^2} f_R + 2 \frac{\partial f_C}{\partial r_{ij}} \frac{\partial f_R}{\partial r_{ij}} + f_C \frac{\partial^2 f_R}{\partial r_{ij}^2} + b_{ij} \left\{\frac{\partial^2 f_C}{\partial r_{ij}^2} f_A + 2 \frac{\partial f_C}{\partial r_{ij}} \frac{\partial f_A}{\partial r_{ij}} + f_C \frac{\partial^2 f_A}{\partial r_{ij}^2}\right\}\right] + \left(\frac{\partial r_{ij}}{\partial \mathbf{x}_i} \frac{\partial b_{ij}}{\partial \mathbf{x}_j} + \frac{\partial b_{ij}}{\partial \mathbf{x}_i} \frac{\partial r_{ij}}{\partial \mathbf{x}_j}\right) \left(\frac{\partial f_C}{\partial r_{ij}} f_A + f_C \frac{\partial f_A}{\partial r_{ij}}\right) + f_C f_A \frac{\partial^2 b_{ij}}{\partial \mathbf{x}_j \partial \mathbf{x}_i}$$

$$\frac{\partial^2 V_{ij}}{\partial \mathbf{x}_j^m \partial \mathbf{x}_j^n} = \frac{\partial^2 r_{ij}}{\partial \mathbf{x}_j^m \partial \mathbf{x}_j^n} \left[\frac{\partial f_C}{\partial r_{ij}} \{f_R + b_{ij} f_A\} + f_C \left\{\frac{\partial f_R}{\partial r_{ij}} + b_{ij} \frac{\partial f_A}{\partial r_{ij}}\right\}\right] + \frac{\partial r_{ij}}{\partial \mathbf{x}_j^m} \frac{\partial r_{ij}}{\partial \mathbf{x}_j^n} \left[\frac{\partial^2 f_C}{\partial r_{ij}^2} f_R + 2 \frac{\partial f_C}{\partial r_{ij}} \frac{\partial f_R}{\partial r_{ij}} + f_C \frac{\partial^2 f_R}{\partial r_{ij}^2} + b_{ij} \left\{\frac{\partial^2 f_C}{\partial r_{ij}^2} f_A + 2 \frac{\partial f_C}{\partial r_{ij}} \frac{\partial f_A}{\partial r_{ij}} + f_C \frac{\partial^2 f_A}{\partial r_{ij}^2}\right\}\right] + \left(\frac{\partial r_{ij}}{\partial \mathbf{x}_j^m} \frac{\partial b_{ij}}{\partial \mathbf{x}_j^n} + \frac{\partial b_{ij}}{\partial \mathbf{x}_j^m} \frac{\partial r_{ij}}{\partial \mathbf{x}_j^n}\right) \left(\frac{\partial f_C}{\partial r_{ij}} f_A + f_C \frac{\partial f_A}{\partial r_{ij}}\right) + f_C f_A \frac{\partial^2 b_{ij}}{\partial \mathbf{x}_j^m \partial \mathbf{x}_j^n}$$

$$\frac{\partial^2 V_{ij}}{\partial \mathbf{x}_j \partial \mathbf{x}_k} = \frac{\partial r_{ij}}{\partial \mathbf{x}_j} \frac{\partial b_{ij}}{\partial \mathbf{x}_k} \left(\frac{\partial f_C}{\partial r_{ij}} f_A + f_C \frac{\partial f_A}{\partial r_{ij}}\right)$$

$$\frac{\partial^2 V_{ij}}{\partial \mathbf{x}_k \partial \mathbf{x}_i} = \frac{\partial r_{ij}}{\partial \mathbf{x}_i} \frac{\partial b_{ij}}{\partial \mathbf{x}_k} \left(\frac{\partial f_C}{\partial r_{ij}} f_A + f_C \frac{\partial f_A}{\partial r_{ij}}\right) + f_C f_A \frac{\partial^2 b_{ij}}{\partial \mathbf{x}_k \partial \mathbf{x}_i}$$

$$\frac{\partial^2 V_{ij}}{\partial \mathbf{x}_k \partial \mathbf{x}_j} = \frac{\partial r_{ij}}{\partial \mathbf{x}_j} \frac{\partial b_{ij}}{\partial \mathbf{x}_k} \left(\frac{\partial f_C}{\partial r_{ij}} f_A + f_C \frac{\partial f_A}{\partial r_{ij}}\right) + f_C f_A \frac{\partial^2 b_{ij}}{\partial \mathbf{x}_k \partial \mathbf{x}_j}$$

$$\frac{\partial^2 V_{ij}}{\partial \mathbf{x}_k \partial \mathbf{x}_k} = f_C f_A \frac{\partial^2 b_{ij}}{\partial \mathbf{x}_k \partial \mathbf{x}_k}$$

Differentiation of  $b_{ij}$  in respect to positions  $\mathbf{x}_i$ ,  $\mathbf{x}_j$ , and  $\mathbf{x}_k$  has same appearance for all cases and expressed as:

$$\frac{\partial^2 b_{ij}}{\partial \mathbf{x}_i^m \partial \mathbf{x}_i^n} = -\frac{1}{2} \beta^n \zeta_{ij}^{n-2} (1 + \beta^n \zeta_{ij}^n)^{-\frac{1}{2n}-2} \left[ (n-1) \frac{\partial \zeta_{ij}}{\partial \mathbf{x}_i^m} \frac{\partial \zeta_{ij}}{\partial \mathbf{x}_i^n} (1 + \beta^n \zeta_{ij}^n) + \zeta_{ij} \frac{\partial^2 \zeta_{ij}}{\partial \mathbf{x}_i^m \partial \mathbf{x}_i^n} (1 + \beta^n \zeta_{ij}^n) + n \beta^n \left(-\frac{1}{2n} - 1\right) \zeta_{ij}^n \frac{\partial \zeta_{ij}}{\partial \mathbf{x}_i^m} \frac{\partial \zeta_{ij}}{\partial \mathbf{x}_i^n} \right]$$

Differentiation of  $\zeta_{ij}$  in respect to positions  $\mathbf{x}_i$ ,  $\mathbf{x}_j$ , and  $\mathbf{x}_k$ :

$$\frac{\partial^2 \zeta_{ijk}}{\partial \mathbf{x}_i^m \partial \mathbf{x}_i^n} = \frac{\partial^2 r_{ik}}{\partial \mathbf{x}_i^m \partial \mathbf{x}_i^n} \frac{\partial f_C}{\partial r_{ik}} g(\theta_{ijk}) + \frac{\partial r_{ik}}{\partial \mathbf{x}_i^m} \frac{\partial r_{ik}}{\partial \mathbf{x}_i^n} \frac{\partial^2 f_C}{\partial r_{ik}^2} g(\theta_{ijk}) + \frac{\partial r_{ik}}{\partial \mathbf{x}_i^m} \frac{\partial f_C}{\partial r_{ik}} \frac{\partial \cos(\theta_{ijk})}{\partial \mathbf{x}_i^n} \frac{\partial g(\theta_{ijk})}{\partial \cos(\theta_{ijk})} + \frac{\partial r_{ik}}{\partial \mathbf{x}_i^n} \frac{\partial f_C}{\partial r_{ik}} \frac{\partial \cos(\theta_{ijk})}{\partial \mathbf{x}_i^m} \frac{\partial g(\theta_{ijk})}{\partial \cos(\theta_{ijk})} + f_C \frac{\partial^2 \cos(\theta_{ijk})}{\partial \mathbf{x}_i^m \partial \mathbf{x}_i^n} \frac{\partial g(\theta_{ijk})}{\partial \cos(\theta_{ijk})} + f_C \frac{\partial \cos(\theta_{ijk})}{\partial \mathbf{x}_i^m} \frac{\partial \cos(\theta_{ijk})}{\partial \mathbf{x}_i^n} \frac{\partial^2 g(\theta_{ijk})}{\partial \cos(\theta_{ijk})^2}$$





$$\frac{\partial^2 \mathbf{r}_{ij} \cdot \mathbf{r}_{ik}}{\partial \mathbf{x}_i^m \partial \mathbf{x}_i^n} = \begin{cases} 2 & \mathbf{x}_i^m = \mathbf{x}_i^n \\ 0 & \mathbf{x}_i^m \neq \mathbf{x}_i^n \end{cases}$$

$$\frac{\partial^2 \mathbf{r}_{ij} \cdot \mathbf{r}_{ik}}{\partial \mathbf{x}_i \partial \mathbf{x}_j} = \begin{cases} -1 & \mathbf{x}_i = \mathbf{x}_j \\ 0 & \mathbf{x}_i \neq \mathbf{x}_j \end{cases}$$

$$\frac{\partial^2 \mathbf{r}_{ij} \cdot \mathbf{r}_{ik}}{\partial \mathbf{x}_i \partial \mathbf{x}_k} = \begin{cases} -1 & \mathbf{x}_i = \mathbf{x}_k \\ 0 & \mathbf{x}_i \neq \mathbf{x}_k \end{cases}$$

$$\frac{\partial^2 \mathbf{r}_{ij} \cdot \mathbf{r}_{ik}}{\partial \mathbf{x}_j \partial \mathbf{x}_i} = \begin{cases} -1 & \mathbf{x}_j = \mathbf{x}_i \\ 0 & \mathbf{x}_j \neq \mathbf{x}_i \end{cases}$$

$$\frac{\partial^2 \mathbf{r}_{ij} \cdot \mathbf{r}_{ik}}{\partial \mathbf{x}_j^m \partial \mathbf{x}_j^n} = 0$$

$$\frac{\partial^2 \mathbf{r}_{ij} \cdot \mathbf{r}_{ik}}{\partial \mathbf{x}_j \partial \mathbf{x}_k} = \begin{cases} 1 & \mathbf{x}_j = \mathbf{x}_k \\ 0 & \mathbf{x}_j \neq \mathbf{x}_k \end{cases}$$

$$\frac{\partial^2 \mathbf{r}_{ij} \cdot \mathbf{r}_{ik}}{\partial \mathbf{x}_k \partial \mathbf{x}_i} = \begin{cases} -1 & \mathbf{x}_k = \mathbf{x}_i \\ 0 & \mathbf{x}_k \neq \mathbf{x}_i \end{cases}$$

$$\frac{\partial^2 \mathbf{r}_{ij} \cdot \mathbf{r}_{ik}}{\partial \mathbf{x}_k \partial \mathbf{x}_j} = \begin{cases} 1 & \mathbf{x}_k = \mathbf{x}_j \\ 0 & \mathbf{x}_k \neq \mathbf{x}_j \end{cases}$$

$$\frac{\partial^2 \mathbf{r}_{ij} \cdot \mathbf{r}_{ik}}{\partial \mathbf{x}_k^m \partial \mathbf{x}_k^n} = 0$$

Differentiation of  $g(\theta_{ijk})$  in respect to  $\cos(\theta_{ijk})$  twice:

$$\frac{\partial^2 g(\theta_{ijk})}{\partial \cos(\theta_{ijk})^2} = \frac{2c^2 \left[ d^2 - 3 \{ h - \cos(\theta_{ijk}) \}^2 \right]}{\left[ d^2 + \{ h - \cos(\theta_{ijk}) \}^2 \right]^3}$$

As for first order differentiation, second order differentiation of  $f_C, f_A, f_R$  in respect to corresponding distance twice should be given.

## References

**Arora, W. J.; Nichol, A. J.; Smith, H. I.; Barbastathis, G.** (2006): Membrane folding to achieve three-dimensional nanostructures: Nanopatterned silicon nitride folded with stressed chromium hinges. *Appl. Phys. Lett.*, vol. 88, pp. 053108–1–3.

**Bhattacharya, P.** (1993): *Properties of Lattice-Matched and Strained Indium Gallium Arsenide*. Institution of Electrical Engineers, London. Chap. 1.2.

**Brenner, D. W.** (1990): Empirical potential for hydrocarbons for use in simulating the chemical vapor deposition of diamond films. *Phys. Rev. B*, vol. 42, pp. 9458–9471.

**Brenner, D. W.; Shenderova, O. A.; Harrison, J. A.; Stuart, S. J.; Ni, B.; Sinnott, S. B.** (2002): A second-generation reactive empirical bond order (REBO) potential energy expression for hydrocarbons. *J. Phys.: Condens. Matter*, vol. 14, pp. 783–802.

**Chirputkar, S. U.; Qian, D.** (2008): Coupled Atomistic/Continuum Simulation based on Extended Space-Time Finite Element Method. *CMES: Computer Modeling in Engineering & Sciences*, vol. 24, no. 3, pp. 185–202.

**Fitzgerald, G.; Goldbeck-Wood, G.; Kung, P.; Petersen, M.; Subramanian, L.; Wescott, J.** (2008): Materials Modeling from Quantum Mechanics to The Mesoscale. *CMES: Computer Modeling in Engineering & Sciences*, vol. 24, no. 3, pp. 169–183.

**Golod, S. V.; Prinz, V. Y.; Mashanov, V. I.; Gutakovsky, A. K.** (2001): Fabrication of conducting GeSi/Si micro- and nanotubes and helical microcoils. *Semicond. Sci. Technol.*, vol. 16, pp. 181–185.

**Hsueh, C.-H.** (2002): Modeling of elastic deformation of multilayers due to residual stresses and external bending. *J. Appl. Phys.*, vol. 91, no. 12, pp. 9652–9656.

**In, H. J.; Kumar, S.; Shao-Horn, Y.; Barbastathis, G.** (2006): Origami fabrication of nanostructured, three-dimensional devices: Electrochemical capacitors with carbon electrodes. *Appl. Phys. Lett.*, vol. 88, pp. 083104–1–3.

**Liu, B.; Huang, Y.; Jiang, H.; Qu, S.; Hwang, K. C.** (2004): The atomic-scale finite element method. *Comput. Methods Appl. Mech. Engrg.*, vol. 193, pp. 1849–1864.

**Liu, B.; Jiang, H.; Huang, Y.; Qu, S.; Yu, M.-F.; Hwang, K. C.** (2005): Atomic-scale finite element method in multiscale computations with

applications to carbon nanotubes. *Phys. Rev. B*, vol. 72, pp. 035435–1–8.

**Nikishkov, G. P.** (2003): Curvature estimation for multilayer hinged structures with initial strains. *J. Appl. Phys.*, vol. 94, no. 8, pp. 5333–5336.

**Nikishkov, G. P.; Khmyrova, I.; Ryzhii, V.** (2003): Finite element analysis of self-positioning microstructures and nanostructures. *Nanotechnology*, vol. 14, pp. 820–823.

**Nikishkov, G. P.; Nishidate, Y.; Ohnishi, T.; Vaccaro, P. O.** (2006): Effect of material anisotropy on the self-positioning of nanostructures. *Nanotechnology*, vol. 17, pp. 1128–1133.

**Nishidate, Y.; Nikishkov, G. P.** (2006): Generalized plane strain deformation of multilayer structures with initial strains. *J. Appl. Phys.*, vol. 100, pp. 113518–1–4.

**Nishidate, Y.; Nikishkov, G. P.** (2007): Effect of thickness on the self-positioning of nanostructures. *J. Appl. Phys.*, vol. 102, pp. 083501–1–5.

**Nordlund, K.; Nord, J.; Frantz, J.; Keinonen, J.** (2000): Strain-induced Kirkendall mixing at semiconductor interfaces. *Comput. Mater. Sci.*, vol. 18, pp. 283–294.

**Schmidt, O. G.; Eberl, K.** (2001): Nanotechnology: Thin solid films roll up into nanotubes. *Nature*, vol. 410, pp. 168.

**Songmuang, R.; Deneke, C.; Schmidt, O. G.** (2006): Rolled-up micro- and nanotubes from single-material thin films. *Appl. Phys. Lett.*, vol. 89, pp. 223109–1–3.

**Tersoff, J.** (1989): Modeling solid-state chemistry: Interatomic potentials for multicomponent systems. *Phys. Rev. B*, vol. 39, pp. 5566–5568.

**Theodosiou, T. C.; Saravanos, D. A.** (2007): Molecular Mechanics Based Finite Element For Carbon Nanotube Modeling. *CMES: Computer Modeling in Engineering & Sciences*, vol. 19, no. 2, pp. 121–134.

**Vaccaro, P. O.; Kubota, K.; Aida, T.** (2001): Strain-driven self-positioning of micromachined structures. *Appl. Phys. Lett.*, vol. 78, no. 19, pp. 2852–2854.